# Studying the fracture surface of brass CuZn37 and aluminum 1100 and their relationship with formability in Single Point Incremental Forming

Marwa K. Qate'a
*Production Engineering and Metallurgy Department, University of Technology, Baghdad, Iraq*
*pme.20.67@grad.uotechnology.edu.iq*

Muhsin J. Jweeg, Adnan I. Mohammed
*Technical Engineering Department, Al-Farahidi University, Baghdad, Iraq. Production Engineering and Metallurgy Department, University of Technology, Baghdad, Iraq*
*muhsin.jweeg@uoalfarahidi.edu.iq, https://orcid.org/0000-0001-7917-9952*
*Adnan.I.Mohammed@uotechnology.edu.iq, https://orcid.org/0000-0002-1097-6512*

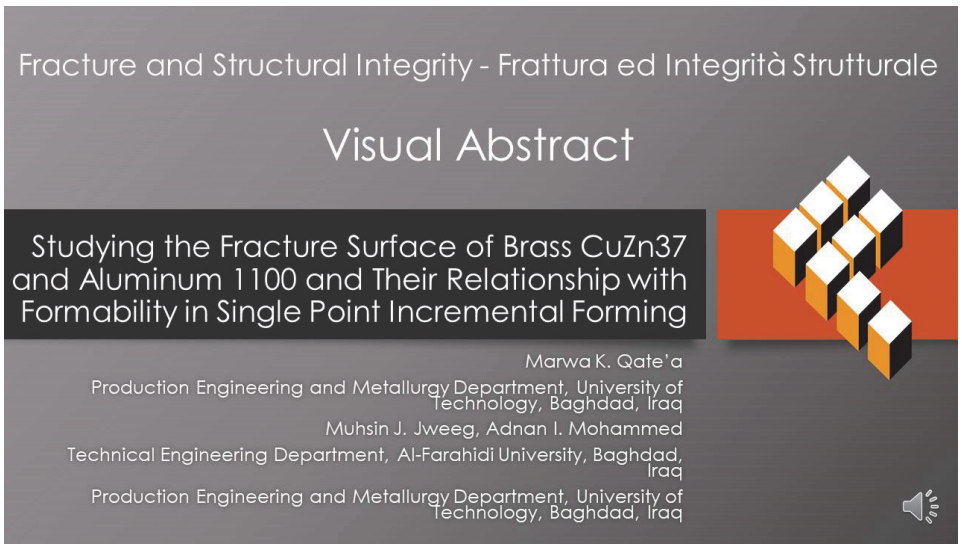


**Citation:** Qate'a; M. K., Jweeg, M. J., Mohammed, A. I., Studying the fracture surface of brass CuZn37 and aluminum 1100 and their relationship with formability in Single Point Incremental Forming, Fracture and Structural Integrity, 72 (2025) 102-120.

**Received:** 13.12.2024
**Accepted:** 02.02.2025
**Published:** 07.02.2025
**Issue:** 04.2025



**KEYWORDS.** SPIF, Fracture surface, Formability, Void Volume Fraction, Void size, Ductile Materials.

## INTRODUCTION

Incremental Sheet Forming (ISF) is un-conventional metal forming operation widely used to create products with complex, free-form shapes without requiring specialized dies. The main components of this process include a sheet metal blank, a backing plate, a blank holder, and a forming tool. The blank holder secures and clamps the metal sheet during forming, while the backing plate supports the sheet to inhibit initial bend and provides an open area for forming. A CNC tool follows a sequence of contours, incrementally deforming the sheet by taking small depth steps

after completing each contour. Single Point Incremental Forming (SPIF) is a broadly adaptable operation that utilizes rapid prototyping techniques to produce small batches of parts economically [1- 4]. Single point incremental forming offers several advantages over conventional sheet metal forming techniques. One of the key benefits is the significant reduction in tooling costs, as SPIF does not require expensive dies or molds and relies on a simple, single tool. This makes it highly cost-effective, especially for low-volume production and rapid prototyping. SPIF also provides exceptional flexibility, allowing for easy customization and design changes by modifying the Computer Aided Design (CAD) file, which shortens lead times compared to traditional methods. SPIF finds applications across various industries, including aerospace, automotive, medical, and architecture. In aerospace, it is used to produce lightweight, complex components like panels and brackets, while in the automotive sector, it aids in prototyping and manufacturing custom or low-volume parts. The medical field benefits from SPIF for creating tailored implants, prosthetics, and surgical instruments [5]. The formability in the SPIF is important because it affects the material's ability to deform without cracking or other defects. The process includes significant strain, so the material must endure this strain without failing. A material's formability largely depends on its properties, such as yield strength, strain hardening, elasticity, anisotropy, and ductility [6, 7]. A primary failure mechanism in ductile metals and alloys includes the growth and coalescence of microscopic voids. These microvoids develop as the material begins to fracture, expanding during plastic deformation and eventually coalescence into larger voids. In the final phase of failure, the voids separate along the surface of this fracture and experience significant necking, leading to a characteristic dimpled pattern. Essentially, the voids form at inclusions and second-phase particles through decohesion of the particle-matrix interface or by particle cracking. The subsequent growth of these voids is driven by plastic deformation in the surrounding matrix [8]. The fracture development process involves the following stages: void nucleation, growth, and coalescence [9].

Generally, the stress/strain conditions and the shape of second-phase particles impact three types of voids: spherical, parabolic, and elliptical. Elliptical voids can be further classified into two types: prolate, which are elongated in the thickness direction, and oblate, which are stretched along the plane of the sheet. The forming conditions affect the type and the number of voids [10]. Various studies by many authors have been developed to investigate the crack surface in the single point incremental forming process; these studies are summarized as follows: K. Ramkumar et al. [11] introduced a novel approach in ISF by using a multipoint tool for SS430 sheets to enhance formability and decrease forming time. They observed that the Multipoint Forming Incremental Process MPIF produced more voids than SPIF, with larger void circumferences in MPIF, indicating better formability with the MPIF tool. Gandhiraj Vignesh et al. [12] evaluated the formability of a 0.8 mm thick SS 202 sheet using both strain-based Forming Limit Diagram (FLD) and stress-based FLD. They observed that the sample with higher formability predominantly exhibited prolate voids, while the other samples mostly showed oblate voids, as identified from the fractographs. Shakir Gatea et al. [13] developed the "Gurson Tvergaard Needleman damage model", which includes stress triaxiality, to forecast ductile fracture in the ISF process caused by void nucleation, growth, and coalescence. Their research revealed that increasing the tool diameter, feed rate and step down can encourage the nucleation of new voids in a pure titanium matrix and speed up the growth of existing ones. Amrut Mulay et al. [1] focused on identifying the most suitable lubricant to improve surface roughness and formability during the ISF of aluminum 5052 H32 sheets. Their findings showed that the breakage zones exhibited large, vast voids and dimples under optimal conditions, suggesting that the fracture occurred at higher plastic strains. Rohit Magdum et al. [14] examined the forming limits and fracture characteristics of AZ31 magnesium alloy components fabricated using the warm incremental sheet forming process. Their results showed that the specimen with the highest formability had a fractured area characterized by prolate voids and a dimpled fracture mode. On the other hand, specimens with medium and low formability displayed prolate voids and exhibited decohesive or cleavage fracture modes on the fractured surface. M. Arun Prasad et al. [15] examined the incremental forming process of thin-rolled cupro-nickel (70/30) alloy sheets using a chrome steel laser-ablated ball. Their findings showed that the cracked surface featured micro-voids, dimples and prolate voids. These prolate voids identified the ductile fracture, which grew toward the sheet's thickness. K. Ramkumar et al. [16] introduced a new multi-point tool to improve the product's final formability and surface finish. They compared its performance with the existing SPIF tool. The Scanning Electron Microscopic (SEM) images of the fractured area produced with the single-point tool revealed more intergranular fractures and facet formations.

Despite extensive research on Single Point Incremental Forming (SPIF), the influence of microstructural void characteristics on formability and fracture behavior remains poorly understood. While prior studies have examined macro-scale formability limits, they often lack detailed void analysis, failing to establish a quantitative correlation between void parameters such as void volume fraction (VVF) and size distribution and formability indicators like fracture depth and maximum wall angle. Comparative studies on different ductile materials remain scarce.

The present work addresses this gap by advancing the understanding of formability in single-point incremental forming by examining the microstructural response of two ductile materials, brass CuZn37 and aluminum 1100, formed into hyperbolic truncated pyramids with varying wall angles until fracture. This study uniquely focuses on correlating formability, measured in terms of fracture depth and maximum wall angle, with specific void characteristics in the fracture zones. These were analyzed through Scanning Electron Microscopy and quantified using ImageJ software. Key innovations in this work include studying the void shapes that formed in each specimen during the SPIF and their relationship with the formability levels. It also identifies the relationship between the formability and the percentage of the void volume fraction VVF, as well as the average void size. This research provides a detailed profile of void distribution, size variation, and implications for material integrity in SPIF by classifying voids into five size categories: very small, small, medium, large, and very large. Furthermore, this work examines how SPIF input parameters influence the relationship between formability and microstructural changes which are represented by VVF and void size in these materials. This level of detail in analyzing void characteristics as indicators of formability and the comparative approach across different materials represents a novel contribution to the field, providing new insights into microstructural effects in incremental sheet forming.

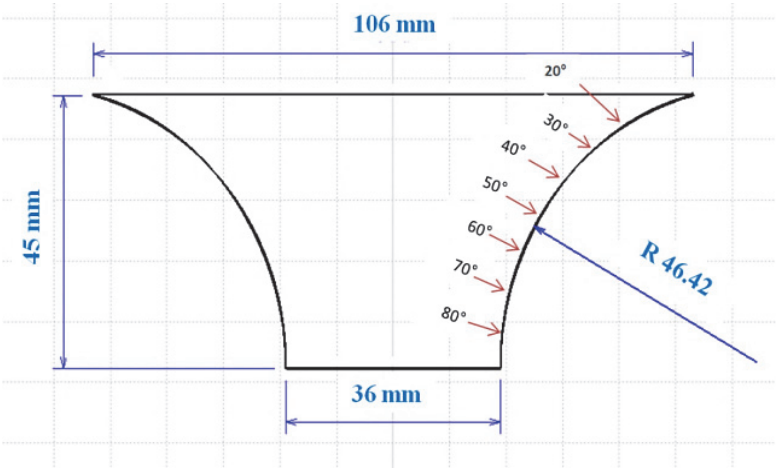


Figure 1: The sketch and dimensions of the formed product (hyperbolic truncated pyramid with varying wall angles).

## MATERIALS AND EXPERIMENTAL WORK

Two types of ductile sheet materials, Brass CuZn37 and Aluminum 1100, with a dimension of 150×150 mm, have been formed by a SPIF process in a hyperbolic truncated pyramid with varying wall angles from 20° to 80° that clarified with dimensions in Fig. 1. The choice of CuZn37 brass and Aluminum 1100 for this study is driven by their industrial significance, differing mechanical properties, and unique microstructural features, all impacting their behavior in Single Point Incremental Forming (SPIF). CuZn37, a two-phase (α+β) brass, exhibits greater strength and strain hardening. In contrast, Aluminum 1100, nearly pure aluminum with a face-centered cubic (FCC) structure, provides enhanced ductility and a more uniform deformation response. These distinctions are expected to affect void formation and fracture mechanisms, making their comparison essential for understanding microstructural influences in SPIF. Aluminum 1100 is likely to achieve greater fracture depth and maximum wall angles due to its superior ductility, while CuZn37, with its heterogeneous grain structure and tendency for strain localization, may develop larger voids and distinct failure patterns. A tensile test of standard specimens was performed using a "Laryee Universal Testing Machine UTM (WDW-50)" per the "ASTM E8M standard" to obtain the mechanical properties of these materials. Fig. 2 depicts the specimens of the ASTM standard used for both ductile materials and Tab. 1 illustrates the mechanical properties of CuZn37 and Al 1100. In order to perform the SPIF process, hemispherical forming tools and the rig have been manufactured, a CAD model for the shape previously illustrated in Fig.1 has been modeled using Solidworks software, and then a z-level tool path has been generated using HSMWORKs software in order to get the G-Codes that entered to the CNC machine. Four input parameters with three levels each for brass CuZn37 material and five input process parameters with three levels each were chosen for aluminum 1100 material. These parameters include feed rate, tool rotation speed, tool diameter, pitch size, and sheet thickness. Tab. 2 lists these key process input parameters and their levels and values. The method that followed to conduct the experiments in this work is based on dividing the

experiments of each material into four groups for brass and five groups for aluminum (A - E). Each group was divided into three experiments to test three levels (low, moderate, and high) of a specific input parameter that affects the formability (where group A used to test the feed rate, group B to test the tool rotation speed, group C to test the tool diameter, group D to test the pitch size, and group E to test the sheet thickness) with keeping the other parameters constant at their moderate level. This method is followed to reach the best level of the tested parameter in each group and use this best level in the rest of the groups. This procedure optimizes the SPIF process and reaches the best parameters that lead to the high formability of aluminum and brass materials. These experimental groups and the design that followed in conducting the experiments are detailed in Tab. 3. These experiments have been conducted using a C-tek model KM-80D three-axis Computer Numerical Control (CNC) vertical milling machine at room temperature with a consistent lubricant, which is PENNZOIL (SAE 5w- 30) lubricant. The fracture depth and maximum wall angle before fracture have been measured as formability indicators of SPIF. Tab. 4 illustrates the results of these experiments.

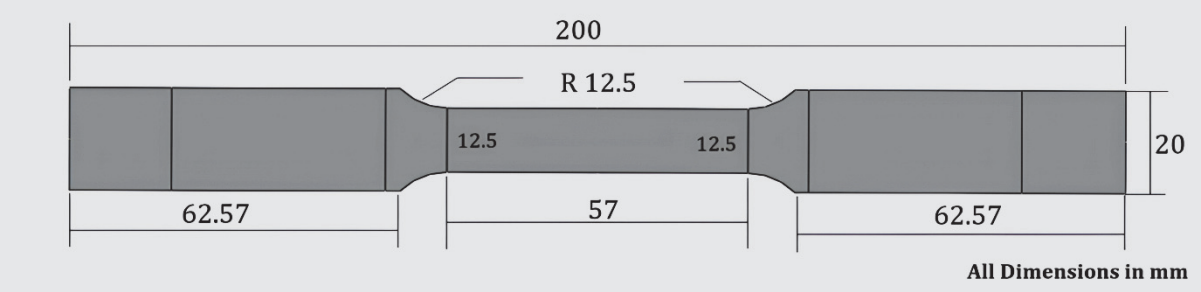


Figure 2: The standard uniaxial tensile specimen per E8/E8M ASTM Standard.

| Mechanical Property | CuZn37 | Al 1100 |
|---|---|---|
| Offset Yield Stress (MPa) | 254 | 152 |
| Tensile Strength (MPa) | 503 | 187 |
| Modulus of Elasticity (GPa) | 97 | 70 |
| Density (g/cm3) [17] | 8.45 | 2.71 |

Table 1: Mechanical properties of brass CuZn37 and aluminum 1100.

| Parameter | Unit | Low Level | Medium Level | High Level |
|---|---|---|---|---|
| Feed rate ($f$) | mm/min | 800 | 1200 | 1600 |
| Tool rotation speed (ω) | rpm | 700 | 1500 | 2300 |
| Tool diameter (D) | mm | 8 | 10 | 12 |
| Pitch Size (z) | mm | 0.3 | 0.7 | 1.1 |
| Thickness (t) | mm | 0.5 | 0.8 | 1 |

Table 2: Key process input parameters with their levels.

| Group A | | | | | |
|---|---|---|---|---|---|
| Exp. No. | Feed rate (mm/min) | Tool rotation speed (rpm) | Tool diameter (mm) | Pitch size (mm) | Sheet thickness (mm) |
| 1 | 800 | | | | |
| 2 | 1200 | 1500 | 10 | 0.7 | 0.8 |
| 3 | 1600 | | | | |
| Group B | | | | | |
| Exp. No. | Feed rate (mm/min) | Tool rotation speed (rpm) | Tool diameter (mm) | Pitch size (mm) | Sheet thickness (mm) |
| 1 | | 700 | | | |
| 2 | Best Level | 1500 | 10 | 0.7 | 0.8 |
| 3 | | 2300 | | | |
| Group C | | | | | |
| Exp. No. | Feed rate (mm/min) | Tool rotation speed (rpm) | Tool diameter (mm) | Pitch size (mm) | Sheet thickness (mm) |
| 1 | | | 8 | | |
| 2 | Best Level | Best Level | 10 | 0.7 | 0.8 |
| 3 | | | 12 | | |
| Group D | | | | | |
| Exp. No. | Feed rate (mm/min) | Tool rotation speed (rpm) | Tool diameter (mm) | Pitch size (mm) | Sheet thickness (mm) |
| 1 | | | | 0.3 | |
| 2 | Best Level | Best Level | Best Level | 0.7 | 0.8 |
| 3 | | | | 1.1 | |
| Group E (Only for Aluminum Sheets) | | | | | |
| Exp. No. | Feed rate (mm/min) | Tool rotation speed (rpm) | Tool diameter (mm) | Pitch size (mm) | Sheet thickness (mm) |
| 1 | | | | | 0.5 |
| 2 | Best Level | Best Level | Best Level | Best Level | 0.8 |
| 3 | | | | | 1.1 |

Table 3: Groups of aluminum and brass material experiments.

| | | Brass CuZn37 | | Aluminum 1100 | |
|---|---|---|---|---|---|
| Group | Exp. No. | Fracture Depth, mm | Wall Angle, ° | Fracture Depth, mm | Wall Angle, ° |
| A | 1 | 34.4 | 76.81 | 37.1 | 80.21 |
| | 2 | 34.4 | 76.81 | 37.1 | 80.21 |
| | 3 | 33.7 | 75.92 | 28 | 68.53 |
| B | 1 | 30.8 | 72.20 | 30.8 | 72.20 |
| | 2 | 34.4 | 76.81 | 37.1 | 80.21 |
| | 3 | 16.4 | 52.13 | 37.1 | 80.21 |
| C | 1 | 21 | 58.88 | 36.4 | 79.33 |
| | 2 | 34.4 | 76.81 | 37.1 | 80.21 |
| | 3 | 19.6 | 56.84 | 35 | 77.57 |
| D | 1 | 25.2 | 64.76 | 36.9 | 79.96 |
| | 2 | 34.4 | 76.81 | 37.1 | 80.21 |
| | 3 | 16.5 | 52.13 | 36.3 | 79.21 |
| E | 1 | - | - | 32.2 | 74 |
| | 2 | - | - | 37.1 | 80.21 |
| | 3 | - | - | 39.2 | 82.38 |

Table 4: Experimental results of the brass and aluminum specimens.

Ten experiments, five brass specimens, which are the specimens: (C-1, B-3, A-3, C-3, and B-1) and five aluminum specimens, which are the specimens: (D-1, B-1, E-1, A-1, and A-3) from Tab. 4, were selected to study the fractured surface of the specimens. This choice was made based on the experiments that showed three different levels of formability: low, moderate, and high formability. Fig. 3 shows these selected experimental specimens with their fracture zones, numbered from 1 to 5 for the brass specimens and from 6 to 10 for the aluminum specimens.

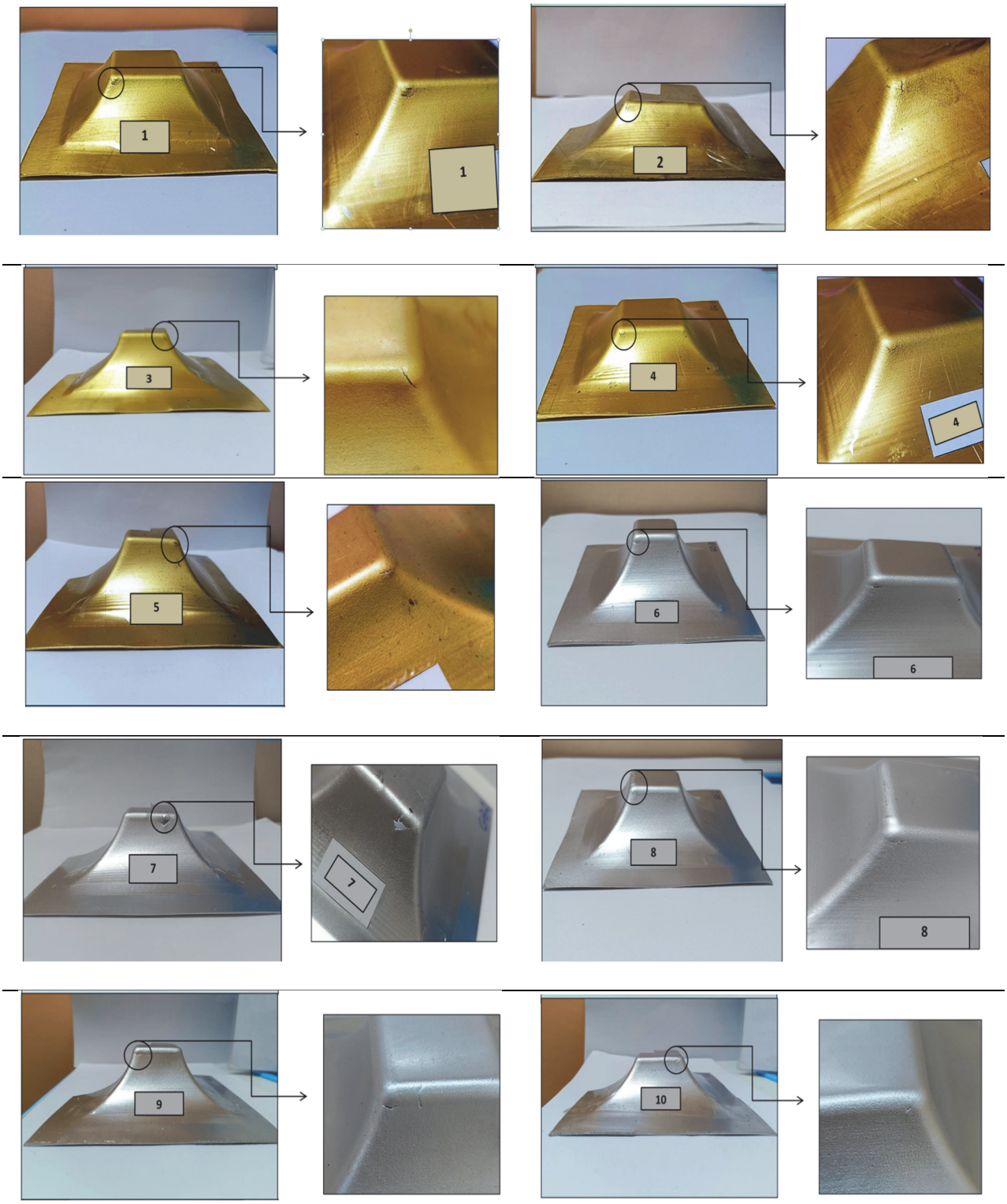


Figure 3: The resulting experimental specimens from the single point incremental forming process with their fracture zones.

## RESULTS AND DISCUSSION

### *Fractography analysis*

Fractography is the study of fractured area to analyze characteristics and relate surface topography to underlying causes or mechanisms of fracture. This analysis often requires detailed examination using a scanning electron microscope (SEM) [18, 19]. In this work, the fractured zones of 10 selected specimens (see Fig. 3) were cut from the whole specimen using wire-cut electrical discharge machining (EDM) after performing single point incremental forming. The fractured surfaces were then examined using SEM (see Fig.s 4 and 5).

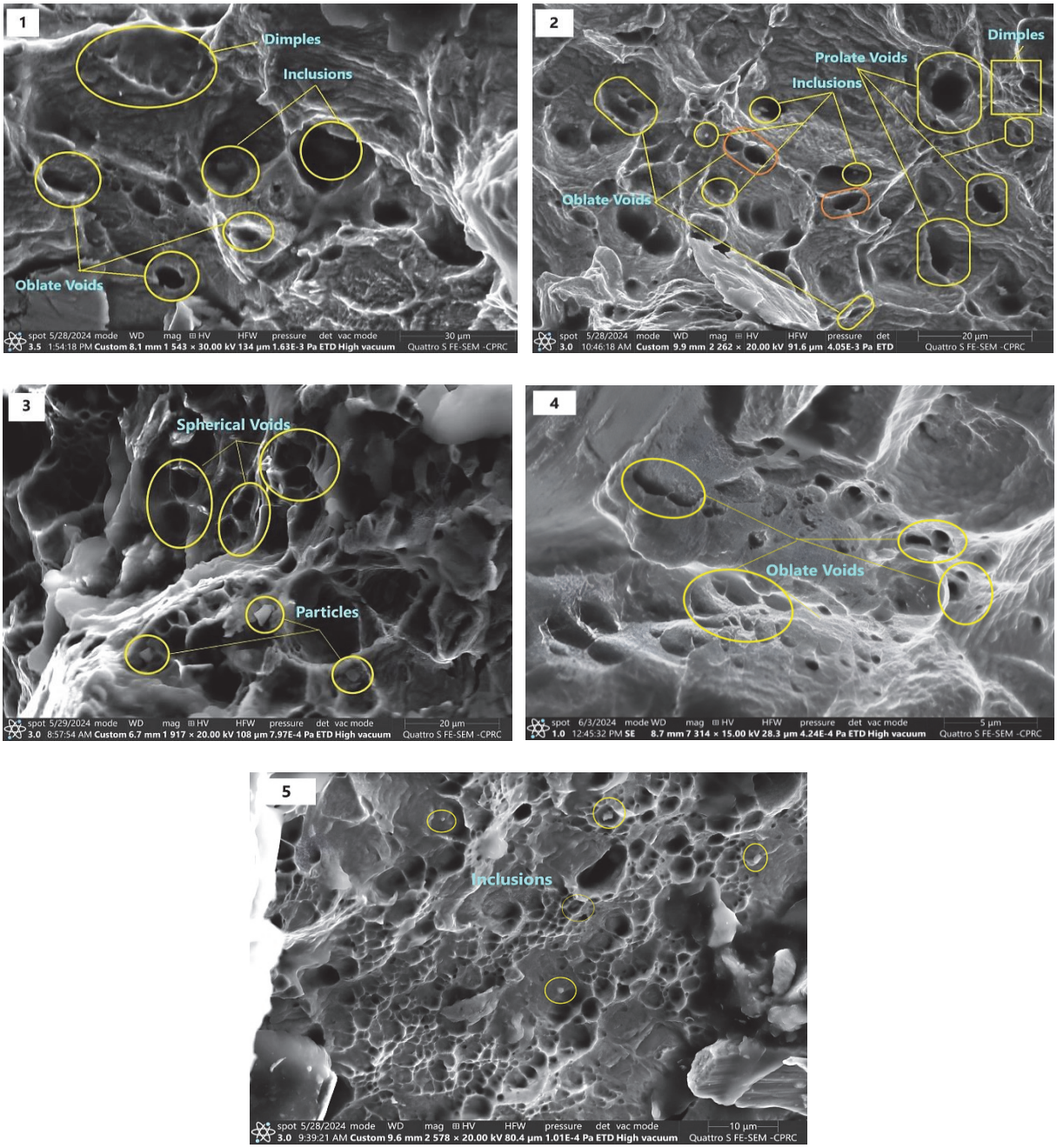


Figure 4: SEM photographs of the fractured surfaces of the specimens of brass CuZn37.

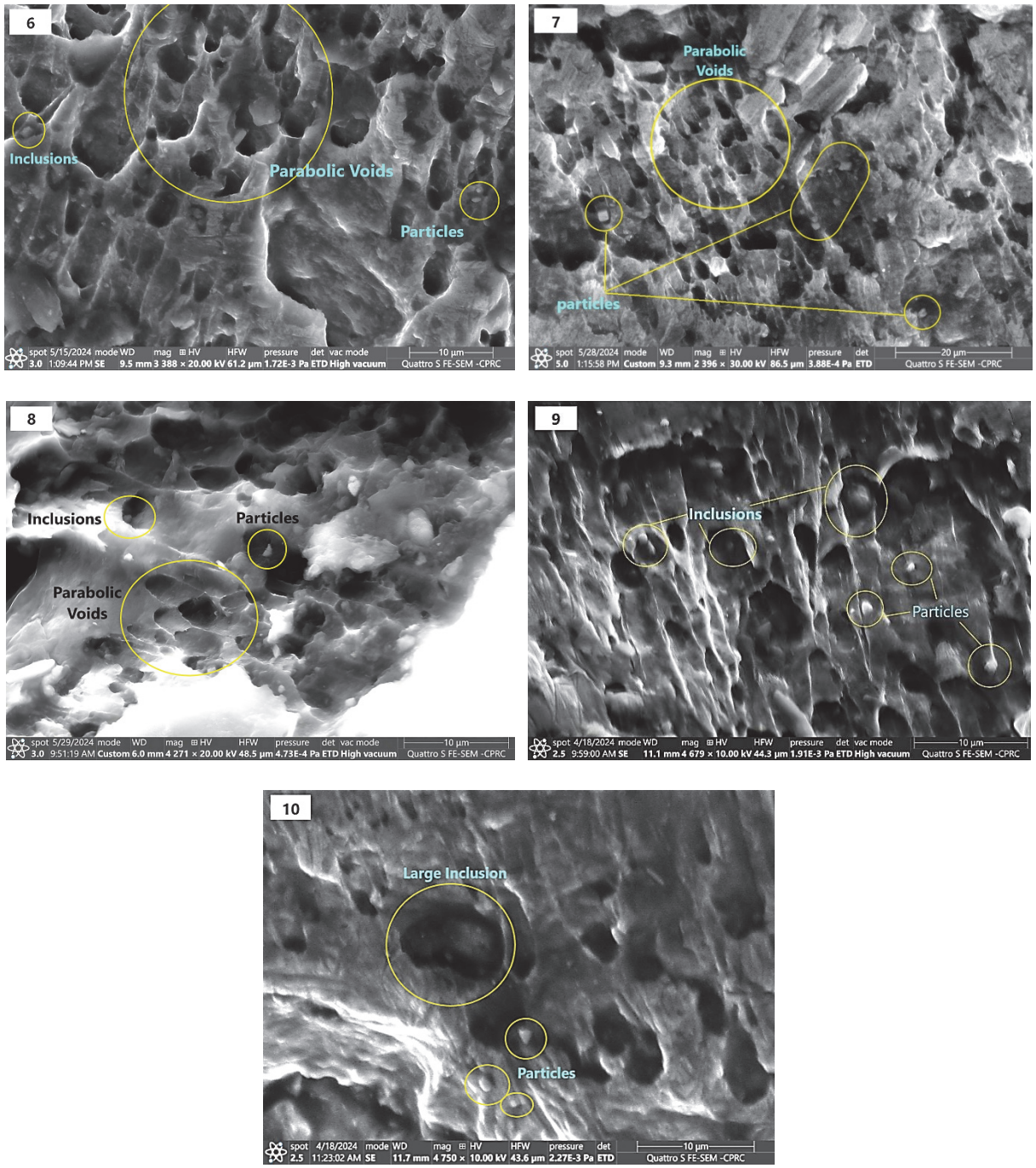


Figure 5: SEM photographs of the fractured surface of the specimens of aluminum 1100.

Figs. 4 and 5 show that the microstructure reveals voids and dimples of varying sizes on the fracture surface, indicating a predominantly ductile fracture. In ductile fractures, damage results from voids' nucleation, growth, and coalescence. Small voids are formed continuously at second-phase particles and non-metallic inclusions across a wide range of plastic strains, eventually leading to material failure. The fracture occurs after significant deformation, known as severe plastic deformation, suggesting that the material underwent a considerable plastic deformation before fracturing. Fig. 4 depicts the SEM photographs of the fracture surface for the five specimens of brass CuZn37 and the analysis of these photographs as follows: In specimen 1, the test program was carried out with a feed rate of 1200 mm/min, a tool rotational speed of 1500 rpm, a tool diameter of 8 mm, a pitch size of 0.7 mm, and a sheet thickness of 0.8 mm, with a fracture depth of 21 mm and maximum wall angle of 58.88°, considering an approximate moderate formability. Many voids in the fracture zone were observed, most flattened in shape and of different sizes, and there were some inclusions

within the voids. All process parameters and the results, sample by sample, are detailed in Tabs. 2 and 3. The results of specimen 2 indicate that its formability is considered relatively low. It was also observed that the fracture contains a large number of voids, both prolate and oblate voids of different sizes, and some inclusions within them. In specimen 3, whose results refer to approximately high formability, it was observed that the majority of voids in the fracture region are spherical voids with different sizes and relatively large numbers, and they also contain some particles. In specimen 4, whose results refer to approximately moderate formability, it was observed that there are a small number of voids in the fractured region and the majority of these voids are oblate voids without any inclusions within them. While the results of specimen 5 indicate that its formability is considered relatively high, and the failure surface has a moderate number of small spherical voids with some inclusions.

Fig. 5 depicts the SEM photographs of the failure surface for the five specimens of aluminum 1100 and the analysis of these photographs as follows: from the results of specimens 6 and 9, which refer to high formability, and the results of specimens 7 and 8, which are considered almost high formability, it was observed that the majority of voids in the fractures of these specimens are parabolic voids, and the gradual difference in these formability is attributed to the differences in sizes and numbers of these voids in each specimen, and it was also observed the presence of some inclusions and particles within them especially in specimen 9. The results in specimen 10 show that the formability ranges between moderate and relatively high. The cracked surface mostly has prolate voids, with one large-sized void and some particles included. The distinct void patterns seen on the fractured surfaces of the brass CuZn37 and aluminum 1100 samples, which are related to their formability, can be attributed to the different deformation behaviors and stress distributions encountered during the incremental forming process.

### *Relationship between formability and microstructure*

ImageJ software was used to analyze the SEM photograph to find the relationship between the formability of ductile materials and their microstructure in each specimen. The SEM images are imported into the software, and the percentage of void volume fraction and the average void size have been calculated. The void volume fraction in the of metals refers to the ratio or percentage of the total area of the fractured surface that is occupied by voids or empty spaces; in other words, it provides a quantitative measure of the void content on this area relative to the total surface area. Mathematically, the void volume fraction can be computed using Eqn. 1.

$$\text{Void Volume Fraction} = \left(\frac{\text{Total area occupied by voids}}{\text{Total area of the surface}}\right) \quad (1)$$

Figs. 6 and 7 show the ImageJ analysis photos of the SEM images for the CuZn37 and Al 1100 crack surfaces, respectively; the black areas refer to the voids present in the fracture area and the white areas refer to the material matrix. The void volume fraction and average void size were measured for each specimen as shown in Tabs. 5 and 6 for CuZn37 and Al 1100 respectively. From these results, it is found that the relationship between the formability of both ductile materials and their percentage of void volume fraction and the average void size is direct; as the average void size increases, the void volume fraction increases, and this leads to increase the formability, which is represented by the depth of fracture and maximum wall angle, this relationship depicts through Figs. 8 and 9 for the specimens of both CuZn37 and Al 1100 materials.

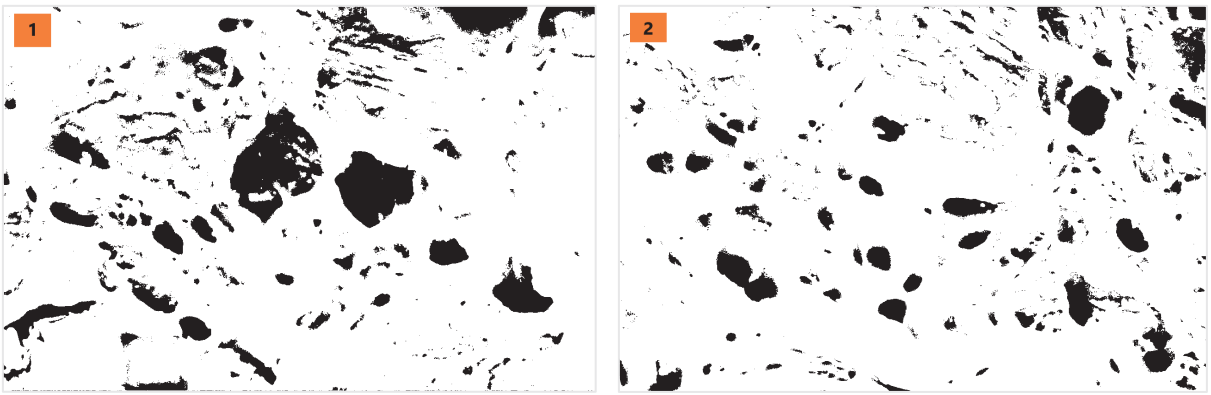

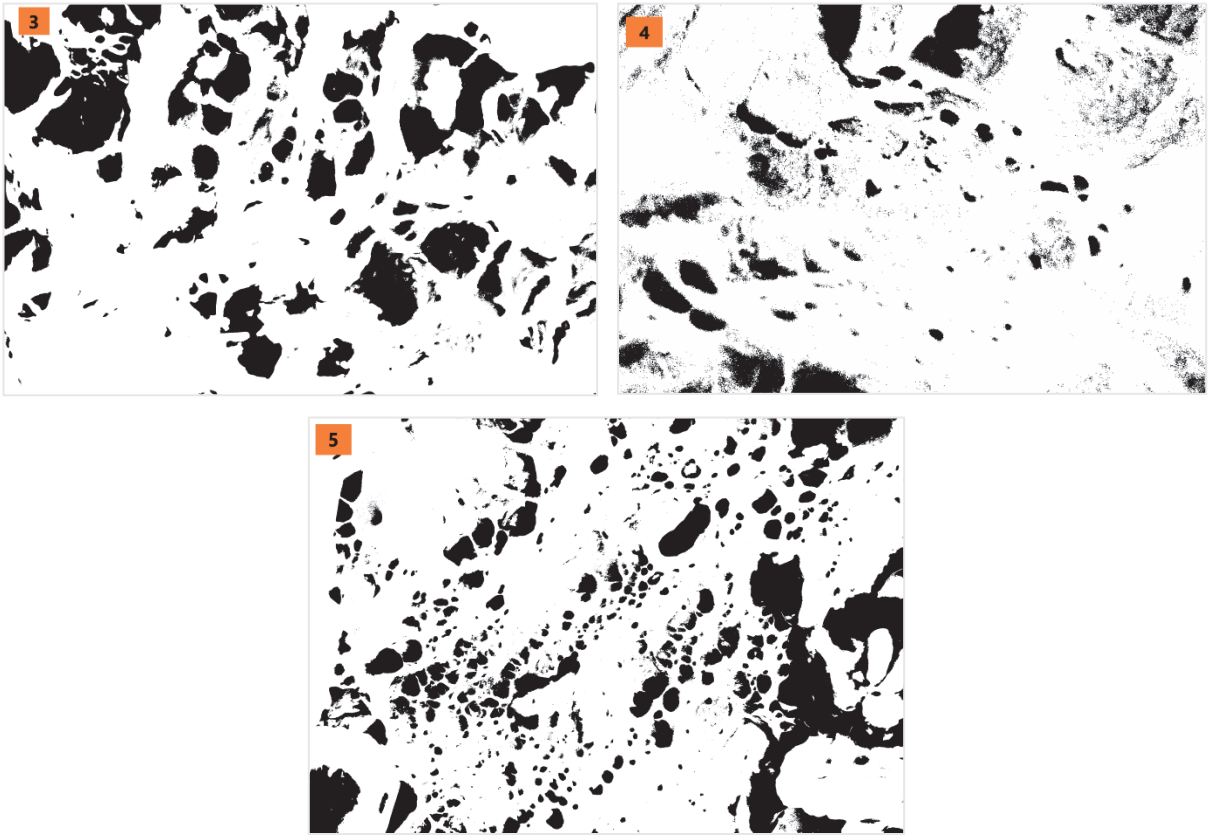


Figure 6: The regions of voids versus the material matrix regions in the cracked surfaces of the specimens of brass CuZn37.

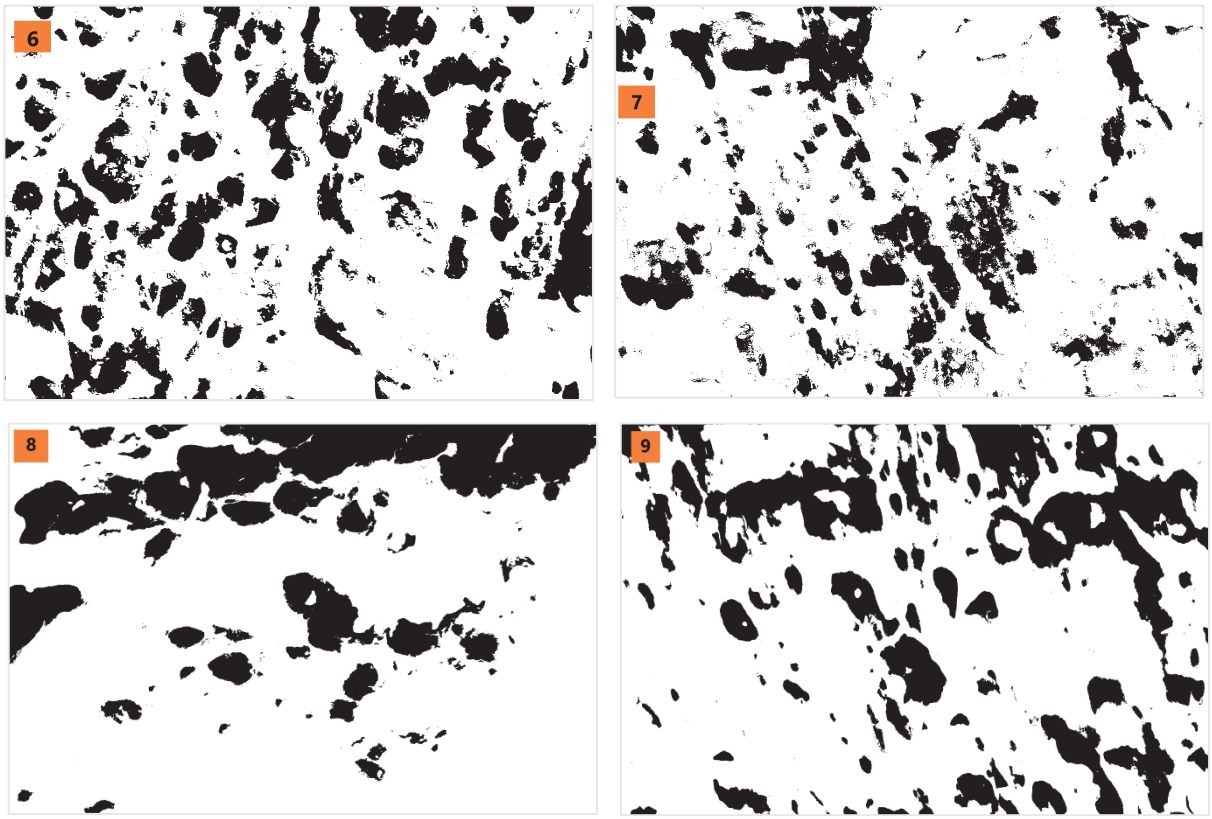

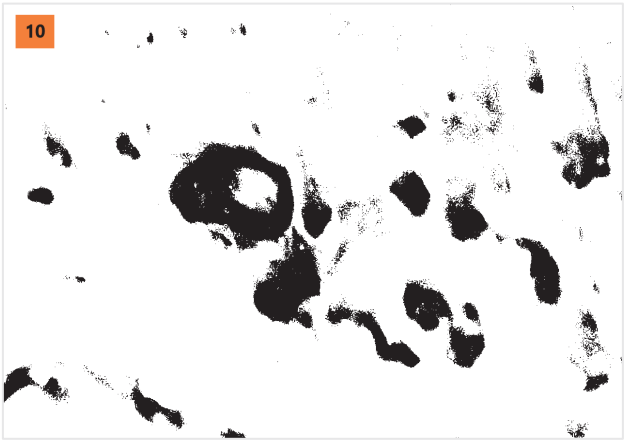


Figure 7: The regions of voids versus the material matrix regions in the cracked surfaces of the specimens of aluminum 1100.

| Specimen | Fracture depth | Maximum wall angle | Void volume fraction | Average void size |
|---|---|---|---|---|
| 1 | 21 mm | 58.88° | 13.82 % | 1.23 µm |
| 2 | 16.4 mm | 52.13° | 9.83 % | 0.44 µm |
| 3 | 33.7 mm | 75.92° | 23.89 % | 1.69 µm |
| 4 | 19.6 mm | 56.84° | 12.30 % | 0.51 µm |
| 5 | 30.8 mm | 72.20° | 23.51 % | 1.37 µm |

Table 5: The analysis results of ImageJ software for the percentage of void volume fraction and the average void size of the brass CuZn37 specimens.

| Specimen | Fracture depth | Maximum wall angle | Void volume fraction | Average void size |
|---|---|---|---|---|
| 6 | 36.3 mm | 79.21° | 25.15 % | 2.08 µm |
| 7 | 30.8 mm | 72.20° | 19.03 % | 1.25 µm |
| 8 | 32.2 mm | 74° | 21.80 % | 1.33 µm |
| 9 | 37.1 mm | 80.21° | 25.62 % | 2.39 µm |
| 10 | 28 mm | 68.53° | 10.61% | 0.69 µm |

Table 6: The analysis results of ImageJ software for the percentage of void volume fraction and the average void size of aluminum 1100 specimens.

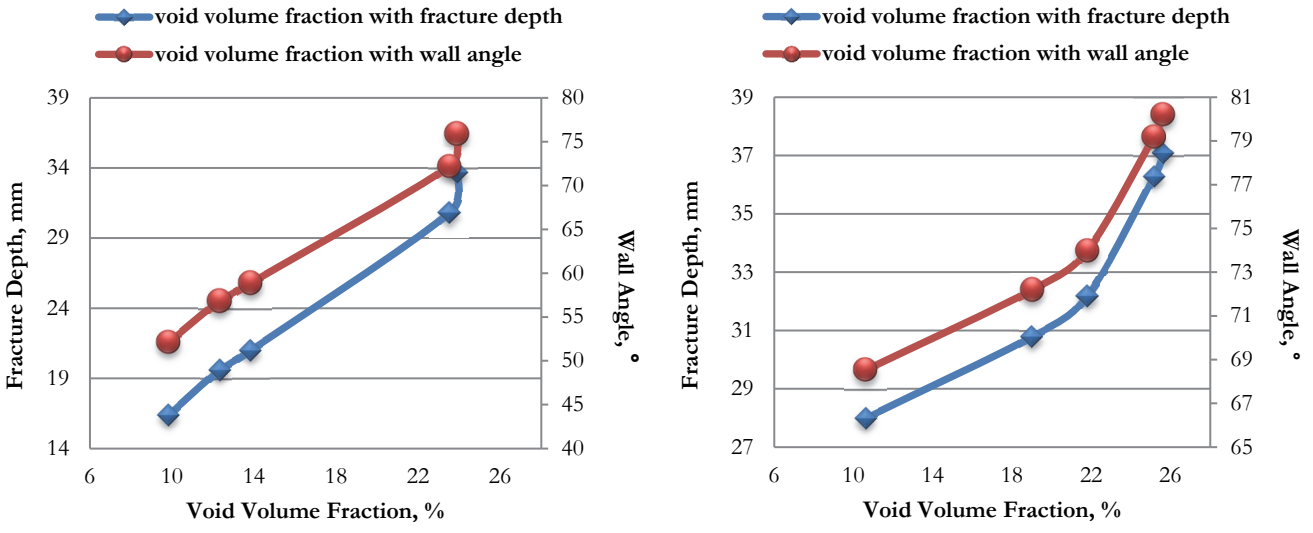


Figure 8: The relationship between the percentage of the void volume fraction and the formability of the specimens of (a) CuZn37 (b) Al 1100.

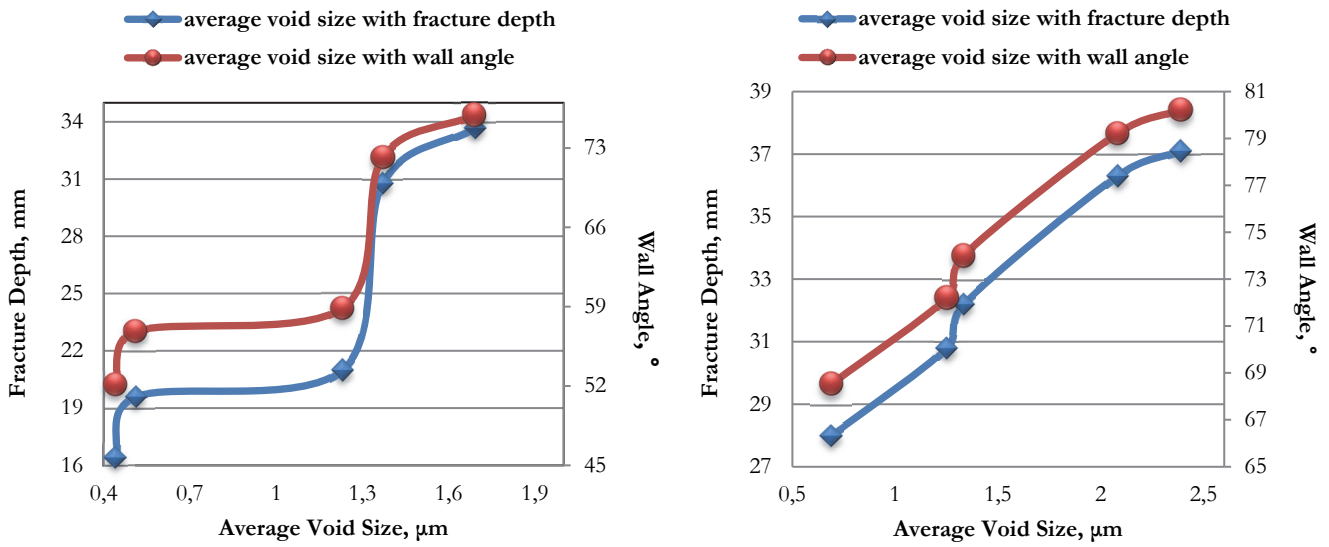


Figure 9: The relationship between the average void size and the formability of the specimens of (a) CuZn37 (b) Al 1100.

*Classification of the Formed Voids*

From the ImageJ software and as previously illustrated in Tabs. 5 and 6, the average void size has been calculated, and the classification of voids that formed during the forming process has been identified for all the specimens of both ductile materials as follows:

For the specimens of brass CuZn37, in the specimen 1, the average void size is 1.23 µm, where the count of voids is 1128, and the maximum and minimum void sizes are 315.2 µm and 0.011 µm, respectively. In specimen 2, the average void size is 0.44 µm, where the count of voids is 1157, and the maximum and minimum void sizes are 38.08 µm and 0.005 µm, respectively. In specimen 3, the average void size is 1.69 µm, where the count of voids is 813, and the maximum and minimum void sizes are 149.7 µm and 0.005 µm, respectively. In specimen 4, the average void size is 0.51 µm, where the count of voids is 51, and the maximum and minimum void sizes are 4.35 µm and 0.085 µm, respectively. In specimen 5, the average void size is 1.37 µm, where the count of voids is 402, and the maximum and minimum void sizes are 25.9 µm and 0.071 µm, respectively. Fig. 10 depicts the five largest void sizes for each specimen of brass CuZn37.

This work has classified the sizes of these voids into five sizes, ranging from very small to very large, according to the classification given below and Tab. 7 illustrates the classification of the voids in each specimen.

0 – 1 µm ⟶ very small
1 – 10 µm ⟶ small
10 – 40 µm ⟶ medium
40 – 75 µm ⟶ large
>=75 µm ⟶ very large

For the specimens of aluminum 1100, in the specimen 6, the average void size is 2.08 µm, where the count of voids is 258, and the maximum and minimum void sizes are 44.98 µm and 0.021 µm, respectively. In specimen 7, the average void size is 1.25 µm, where the count of voids is 626, and the maximum and minimum void sizes are 102.8 µm and 0.019 µm, respectively. In specimen 8, the average void size is 1.33 µm, where the count of voids is 93, and the maximum and minimum void sizes are 27 µm and 0.007 µm, respectively. In specimen 9, the average void size is 2.39 µm, where the count of voids is 49, and the maximum and minimum void sizes are 15.35 µm and 0.255 µm, respectively. In specimen 10, the average void size is 0.69 µm, where the count of voids is 200, and the maximum and minimum void sizes are 43.7 µm and 0.008 µm, respectively. Fig. 11 depicts the five largest void sizes for each specimen of aluminum 1100, and Tab. 8 illustrates the classification of the voids in each specimen.

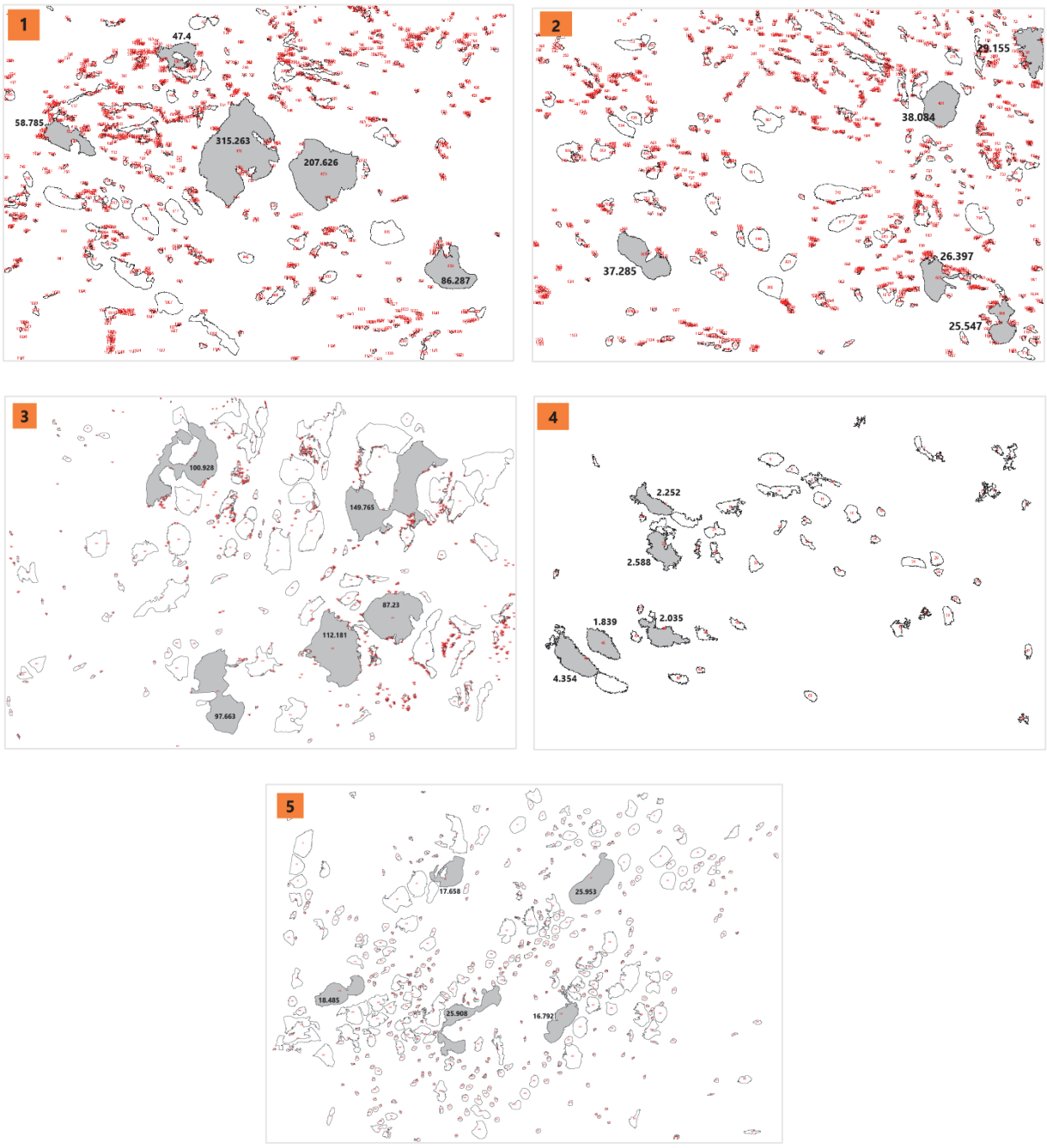


Figure 10: The largest void sizes in each specimen of brass CuZn37.

| Specimen | Total Count | Very small | | Small | | Medium | | Large | | Very Large | |
|---|---|---|---|---|---|---|---|---|---|---|---|
| Specimen 1 | 1128 | 1025 | 90.86 % | 85 | 7.53 % | 12 | 1.06 % | 3 | 0.26 % | 3 | 0.26 % |
| Specimen 2 | 1157 | 1083 | 93.60 % | 63 | 5.40 % | 11 | 1.01 % | 0 | 0 % | 0 | 0 % |
| Specimen 3 | 813 | 731 | 89.90 % | 52 | 6.39 % | 22 | 2.70 % | 3 | 0.36 % | 5 | 0.61 % |
| Specimen 4 | 51 | 46 | 90.19 % | 5 | 9.80 % | 0 | 0 % | 0 | 0 % | 0 | 0 % |
| Specimen 5 | 402 | 292 | 72.63 % | 104 | 25.87 % | 6 | 1.49 % | 0 | 0 % | 0 | 0 % |

Table 7: Classification of voids in the specimens of brass cuzn37.

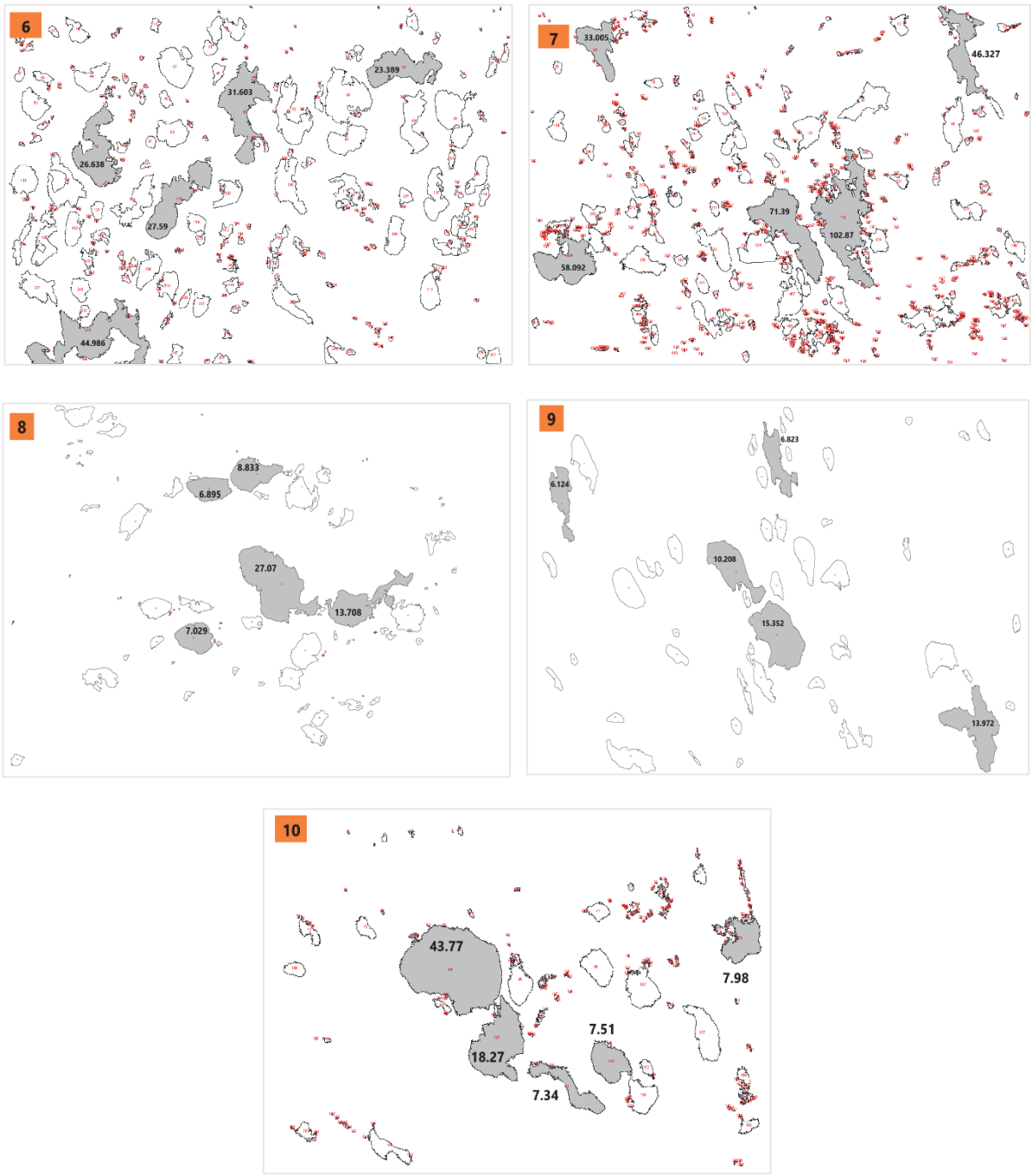


Figure 11: The largest void sizes in each specimen of aluminum 1100.

| Specimen | Total Count | Very small | | Small | | Medium | | Large | | Very Large | |
|---|---|---|---|---|---|---|---|---|---|---|---|
| Specimen 6 | 258 | 187 | 72.48 % | 56 | 21.70 % | 14 | 5.42 % | 1 | 0.38 % | 0 | 0 % |
| Specimen 7 | 626 | 553 | 88.33 % | 55 | 8.78 % | 14 | 2.23 % | 3 | 0.47 % | 1 | 0.15 % |
| Specimen 8 | 93 | 70 | 75.26 % | 21 | 22.58 % | 2 | 2.15 % | 0 | 0 % | 0 | 0 % |
| Specimen 9 | 49 | 25 | 51.02 % | 21 | 42.85 % | 3 | 6.12 % | 0 | 0 % | 0 | 0 % |
| Specimen 10 | 200 | 182 | 91 % | 16 | 8 % | 1 | 0.50 % | 1 | 0.50 % | 0 | 0 % |

Table 8: Classification of voids in the specimens of aluminum 1100.

*Effect of the Input Parameters on the relationship between Formability and Microstructure*

Results obtained in Tabs. 4, 5 and 6 indicate a direct relationship between both formability and VVF with void size, which was obtained previously. The relationship between formability and VVF percentage with the effect of the SPIF parameters is as follows:

For the specimens of brass CuZn37, in specimens 1 and 4, as the formability is almost moderate, with a fracture depth and maximum wall angle of 21 mm, 58.88° and 19.6 mm, 56.84°, respectively, and with a VVF percentage of 13.82 % and 12.30 %, respectively. This is due to the effect of tool diameter, which in these specimens is 8 mm (low level) and 12 mm (high level), respectively. It affects the SPIF process as follows: the formability and the VVF percentage increase when the diameter of the tool increases between 8 mm and 10 mm, i.e., from the low to the medium level, but when the diameter of the tool increases between 10 mm and 12 mm, i.e., from the medium to the high level, the formability and VVF percentage decreases. All specimens' results, sample by sample, are detailed in Tabs. 5 and 6. In specimen 2, as the formability is relatively low, and in contrast, in specimen 5, as the formability is relatively high, this result is due to the effect of tool rotation speed; in these specimens, the tool rotation speed is 2300 rpm (high level) and 700 rpm (low level), respectively. This parameter has an impact on the SPIF process as follows: the formability and the VVF percentage are increased when the tool rotation speed increases between 700 rpm and 1500 rpm, i.e., from the low to the medium level, but when the tool rotation speed increases between 1500 mm and 2300 mm, i.e., from the medium to the high level, the formability and VVF percentage decreased. As the formability is considered almost high in specimen 3, the reason for this result is that the effect feed rate, which in this specimen is 1600 mm (high level), parameter affects the SPIF process as follows: when the feed rate increases from 800 mm to 1200 mm, i.e., from the low to the medium level, the formability and the VVF percentage stay constant in their high values, and despite that the increasing of feed rate from 1200 mm to 1600 mm, i.e., from the medium level to the high level leads to slightly decrease the formability and VVF percentage but it remains considered high.

For the specimens of aluminum 1100, in specimen 6, the formability is considered high due to the effect of the step size, which is 1.1 mm (high level). This parameter has an impact on the SPIF process as follows: when the step size increases between 0.3 mm and 0.7 mm, i.e., from the low to the medium level, the formability and the VVF percentage slightly increase, but when step size increases from 0.7 mm to 1.1 mm, i.e., from the medium to the high level, the formability and VVF percentage decrease somewhat, but in general, in the three experiments that test the effect of step size, the formability and hence the VVF remain high. In specimen 7, the formability is almost high, this is because of the effect of the tool rotation speed, which in this specimen is 700 rpm (low level) and it is affects the SPIF process as follows: when the tool rotation speed increases between 700 rpm and 1500, i.e., from the low to the medium level, the formability and the VVF percentage are increased, but when tool rotation speed increased between 1500 rpm and 2300 rpm, i.e., from the medium to the high level, the formability and VVF percentage keep constant in their high values. In specimen 8, the formability is almost high, and this result is returned to the effect of the sheet thickness, which is 0.5 mm (low level) in this specimen. This parameter has an impact on the SPIF process as follows: when the sheet thickness increases between 0.5 mm and 0.8 mm, i.e., from the low to the medium level, the formability and the VVF percentage are increased, but when sheet thickness increases from 0.8 mm to 1 mm, i.e., from the medium to the high level, the formability and VVF percentage is increased more. In specimen 9, the formability is high; in contrast, in specimen 10, the formability tends to be between moderate and relatively high, and this result is due to the effect of the feed rate in these specimens, which are 1200 mm (medium level) and 1600 mm (high level), respectively. This parameter affects the SPIF process as follows: the formability and the VVF percentage stay constant in their high values when the feed rate increases from 800 mm to 1200, i.e., from the low to the medium level, while the formability and the VVF percentage decreases as the feed rate increases from 1200 mm to 1600 mm, i.e., from the medium to the high level.

*Statistical Analysis*

The statistical analysis of the measured outputs (formability and void characteristics) for both ductile materials brass CuZn37 and aluminum 1100 has been performed to enhance the reliability of the results. The confidence interval is a range of values calculated from sample data likely to include the true population parameter (like a population mean or proportion). It helps assess the uncertainty or variability of the sample statistic; this can be calculated using Eqns. 2 and 3.

$$\text{Confidence Interval (CI)} = \bar{X} \pm MOE \tag{2}$$

$$\text{Margin of Error (MOE)} = Z \times \left(\frac{s}{\sqrt{n}}\right) \tag{3}$$

where $\bar{X}$: the mean of data, Z: the critical t-value, s: the standard deviation, n: the sample size. And by using excel these parameters have been calculated from the following functions: Mean of data ($\bar{X}$) =AVERAGE(range), Standard deviation (s) =STDEV.S(range), Sample size (n) =COUNT(range), Margin of Error (MOE) =CONFIDENCE.T(1-0.95,standard_dev,size) [20].

The results of the lower and upper confidence interval of the formability (fracture depth and maximum wall angle) and void characteristics (void volume fraction and void size) for the both materials have been illustrated in Tabs. 9 and 10, respectively.

| Statistical Analysis | Formability | | Void Characteristics | |
|---|---|---|---|---|
| | Fracture depth | Maximum wall angle | Void volume fraction | Void size |
| Mean | 24.3 | 62.594 | 16.67 | 1.048 |
| Stdev. | 7.516648189 | 10.69508205 | 6.57493346 | 0.549563463 |
| Count | 5 | 5 | 5 | 5 |
| MOE | 9.333151444 | 13.27969834 | 8.163858168 | 0.682373167 |
| Minimum | 16.4 | 52.13 | 9.83 | 0.44 |
| Maximum | 33.7 | 75.92 | 23.89 | 1.69 |
| Lower CI (95%) | 14.96684856 | 49.31430166 | 8.506141832 | 0.365626833 |
| Upper CI (95%) | 33.63315144 | 75.87369834 | 24.83385817 | 1.730373167 |

Table 9: Statistical analysis of the formability and void characteristics results of brass CuZn37.

| Statistical Analysis | Formability | | Void Characteristics | |
|---|---|---|---|---|
| | Fracture depth | Maximum wall angle | Void volume fraction | Void size |
| Mean | 32.88 | 74.83 | 20.442 | 1.548 |
| Stdev. | 3.811430178 | 4.884275791 | 6.113163665 | 0.682729815 |
| Count | 5 | 5 | 5 | 5 |
| MOE | 4.732515633 | 6.064629407 | 7.590495238 | 0.847721032 |
| Minimum | 28 | 68.53 | 10.61 | 0.69 |
| Maximum | 37.1 | 80.21 | 25.62 | 2.39 |
| Lower CI (95%) | 28.14748437 | 68.76537059 | 12.85150476 | 0.700278968 |
| Upper CI (95%) | 37.61251563 | 80.89462941 | 28.03249524 | 2.395721032 |

Table 10: Statistical analysis of the formability and void characteristics results of aluminum 1100.

### *Summary of results*

The experimental findings provided significant insights into the fracture behavior and formability of brass (CuZn37) and aluminum (Al 1100) under various incremental sheet forming (ISF) conditions. Fracture surface analysis showed that both materials underwent ductile fracture mechanisms involving void nucleation and growth. Furthermore, a correlation between formability and void volume fraction (VVF) was established, illustrating how process parameters such as tool diameter, rotation speed, feed rate, step size, and sheet thickness affected the material's deformation behavior. To

summarize these findings comprehensively, Tab. 11 offers a detailed comparison of the key observations, emphasizing the impact of different process parameters on formability, VVF, void morphology, and failure mechanisms.

| Aspect | Main Findings |
|---|---|
| Fracture behavior | 1. Both brass CuZn37 and aluminum 1100 exhibited ductile fracture with void nucleation, growth, and coalescence.<br>2. Fracture surfaces contained dimples, confirming plastic deformation before failure. |
| Formability & void volume fraction relationship | 1. Direct relationship observed between formability and void characteristics.<br>2. As average void size increased, VVF increased, leading to higher formability (measured by fracture depth and maximum wall angle). |
| Effect of tool diameter (CuZn37) | 1. Tool diameter significantly influenced formability and VVF.<br>2. Increase from 8 mm to 10 mm leads to higher formability and VVF.<br>3. Further increase from 10 mm to 12 mm leads to decrease in formability and VVF. |
| Effect of tool rotation speed (CuZn37 & Al 1100) | 1. Increase from 700 rpm to 1500 rpm leads to higher formability and VVF.<br>2. Further increase to 2300 rpm leads to decrease in formability and VVF. |
| Effect of feed rate (CuZn37 & Al 1100) | 1. Lower feed rates (800–1200 mm/min) leads to higher formability and VVF.<br>2. Increase from 1200 mm/min to 1600 mm/min leads to slight reduction in formability and VVF. |
| Effect of step size (Al 1100) | 1. Increase from 0.3 mm to 0.7 mm leads to slight increase in formability and VVF.<br>2. Further increase to 1.1 mm leads to slight decrease in formability, but VVF remained relatively high. |
| Effect of sheet thickness (Al 1100) | 1. Increase from 0.5 mm to 0.8 mm leads to simproved formability and VVF.<br>2. Further increase to 1 mm leads to continued improvement in formability and VVF. |
| Void shape analysis (CuZn37 & Al 1100) | 1. CuZn37 specimens displayed spherical, oblate, and prolate voids, depending on process parameters.<br>2. Aluminum 1100 specimens primarily exhibited parabolic voids.<br>3. Differences in void shapes contributed to variations in formability. |
| Failure surface analysis (CuZn37 & Al 1100) | 1. SEM analysis showed variations in void distribution across specimens.<br>2. CuZn37 fracture surfaces had different void patterns, influenced by tool parameters.<br>3. Aluminum 1100 surfaces contained inclusions and particles within voids, especially in higher formability samples. |

Table 11: Summary of the main results.

## CONCLUSIONS

This work investigated the formability and fracture characteristics of two ductile materials, brass CuZn37 and aluminum 1100, formed into hyperbolic truncated pyramids through single-point incremental forming (SPIF) until failure. The fractured surfaces were analyzed using SEM and ImageJ software to evaluate void morphology.

1. In the brass CuZn37 specimens, void formation varied with formability. Oblate voids were predominant in specimens with moderate formability, while spherical voids appeared in those with relatively high formability. A combination of oblate and prolate voids was observed in specimens with lower formability. Similarly, aluminum 1100 exhibited distinct void shapes, with parabolic voids forming in high-formability specimens and prolate voids in specimens with moderate-to-high formability.
2. A direct relationship was found between formability, represented by fracture depth and maximum wall angle, and void characteristics, such as volume fraction and average void size. Higher void volume fractions and larger void sizes were associated with increased formability in CuZn37 and Al 1100.
3. The void volume fraction ranged from 9.83% to 23.89% in CuZn37 and 10.61% to 25.62% in Al 1100, with maximum average void sizes of 1.69 μm and 2.39 μm, respectively.
4. The average void sizes in the fractured surfaces of CuZn37 range from a maximum of 1.69 μm to a minimum of 0.44 μm, whereas in Al 1100, they range from 2.39 μm to 0.69 μm.

5. The largest void sizes observed in the five CuZn37 specimens are 315.2 μm, 38.08 μm, 149.7 μm, 4.35 μm, and 25.9 μm, respectively. Similarly, in Al 1100 specimens, the largest void sizes recorded are 44.98 μm, 102.8 μm, 27 μm, 15.35 μm, and 43.7 μm, respectively.
6. The study identified the optimal SPIF conditions to enhance formability. In brass CuZn37, the void volume fraction was maximized when all input parameters were set to medium levels. In aluminum 1100, optimal conditions were achieved with a low feed rate, high tool rotation speed and sheet thickness, and medium tool diameter and step size. These findings provide valuable insights into the role of void morphology in SPIF and contribute to understanding formability enhancement in ductile materials.

   The findings of this study have practical implications for industries utilizing SPIF, particularly in sectors such as aerospace, automotive, and biomedical engineering, where forming ductile materials like brass CuZn37 and aluminum 1100 is crucial. Manufacturers can enhance material formability by optimizing process parameters—such as feed rate, tool rotation speed, and step size, reducing defects and improving product reliability. For instance, in automotive prototyping, improved formability can facilitate the production of complex sheet metal components with fewer fractures, minimizing material waste and machining costs. Controlling void formation can enhance mechanical performance and longevity in biomedical applications, such as patient-specific implants made from aluminum alloys. These insights contribute to advancing SPIF as a more efficient, cost-effective, and sustainable manufacturing technique for low-volume and customized production.

## ACKNOWLEDGMENT

The authors would like to thank Dr. Shakir Gatea from the University of Nottingham for his scientific support for this work.

## REFERENCES

[1] Amrut, M., Satish, B. and Ismail S. (2020). Lubricant selection and post forming material characterization in incremental sheet forming, IOP Conf. Series: Materials Science and Engineering, 967(012072). DOI: 10.1088/1757-899X/967/1/012072.

[2] Nguyen, T.N., Nguyen, H.H., Nguyen T.H., Tran T.H. and Ho, H.H. (2021). A research on the formability of pvc sheet in single point incremental forming (SPIF) technology, E3S Web of Conferences, 327(05005). DOI: 10.1051/e3sconf/202132705005.

[3] Tyler, J.G., Filipe C. and Ihab R. (2023). Numerical investigation of step size effect on formability of 2024-t3 aluminum in incremental forming, Journal of Manufacturing and Materials Processing, 7 (2). DOI: 10.3390/jmmp7020070.

[4] Maheshwar, D. and Vinayak, K. (2019). The effect of process parameters on forming forces in single point incremental forming, Procedia Manufacuring, 18th International Conference on Sheet Metal, 29, pp. 120 –128, DOI: 10.1016/j.promfg.2019.02.116.

[5] Premika, S. (2013). Single point incremental forming and multi-stage incremental forming on aluminum alloy 1050, PhD thesis, Universidade do Porto.

[6] Trzepiecinski, T. (2020). Tribological performance of environmentally friendly bio-degradable lubricants based on a combination of boric acid and bio-based oils, Materials, 13(17). DOI: 10.3390/ma13173892.

[7] Yaroslav, E., Sergei, S., Ilya, P. and Aleksandr, K. (2023). An advanced method to test the formability in single point incremental forming. AIP Conf. Proc., proceedings of the iv international scientific conference on advanced technologies in aerospace, mechanical and automation engineering: (MIST: Aerospace-IV 2021), Krasnoyarsk, Russian, 2700(1). DOI: 10.1063/5.0124949.

[8] Amine B.A. and Jean-Baptiste L. (2010). Ductile fracture by void growth to coalescence, Advances in Applied Mechanics, 44, pp. 169-305. DOI: 10.1016/S0065-2156(10)44003-X.

[9] George, A.P. (2019). A short review on fracture mechanisms of mechanical components operated under industrial process conditions: fractographic analysis and selected prevention strategies, Metals, 9(148). DOI: 10.3390/met9020148.

[10] Narayanasamy R., Parthasarathi, N.L., Sathiya N.C. (2009), Effect of microstructure on void nucleation and coalescence during forming of three different HSLA steel sheets under different stress conditions, Materials and Design, 30(4), pp. 1310–1324. DOI: 10.1016/j.matdes.2008.06.043.

[11] Ramkumar, K., Paulraj, G., Elangovan, K. and Sathiya N.C. (2018). Forming limit diagram, void analysis, strain distribution and surface roughness for ss430 sheets during multipoint incremental forming, Arch. Metall. Mater. 63(4), pp. 1709-1714. DOI: 10.24425/amm.2018.125096.

[12] Vignesh, G., Sathiya N.C., Pandivelan, C., Shanmugapriya, K., Bhavishya N.T. and Lavuri, T. (2019). Forming, fracture and corrosion behaviour of stainless steel 202 sheet formed by single point incremental forming process, Materials Research Express, 6(12). DOI: 10.1088/2053-1591/ab5606.

[13] Shakir, G., Bin, L., Jun, C., Hengan, O. and Graham, M. (2019). Investigation of the effect of forming parameters in incremental sheet forming using a micromechanics based damage model, International Journal of Material Forming, 12, pp. 553–574. DOI: 10.1007/s12289-018-1434-3.

[14] Magdum, R., Chinnaiyan, P. (2023). Experimental investigation and optimization of az31 mg alloy during warm incremental sheet forming to study fracture and forming behavior, Coatings, 13(68). DOI: 10.3390/coatings13010068

[15] Arun, P.M., Chinnaiyan, S. N. and Varatharajulu, M. (2024). Improvement of formability and surface finish of cupro-nickel (70/30) alloy during single point incremental forming process using chrome steel laser ablated ball, Surface Review and Letters, 31(8). DOI: 10.1142/S0218625X24500616.

[16] Ramkumar, K., Selvarajan, K.A., Sathiya N.C. and Bovas, H.B.A. (2024). Performance analysis of multi-point incremental forming tool using martensitic AISI 420 sheet metals, Archives of Metallurgy and Materials, 69(1), pp. 325-336. DOI: 10.24425/amm.2024.149097.

[17] Annual Book of ASTM Standards, (2010), USA, Library of Congress Catalog Card Number: 83-641658, ISBN 978-0-8031-8160-1(set), ISBN 978-08031-8352-0 (volume), Printed in Baltimore, MD.

[18] Hiyam, F. (2021). Chapter 9 - failure analysis, operation, maintenance, and repair of land-based gas turbines, Italy, Elsevier, pp. 197-221. DOI: 10.1016/C2019-0-02860-9.

[19] Gopal Krishna U.B.,Vasudeva, B., Virupaxi A. and Madeva N. (2022). Mechanical characterization and tensile fractography of Al7075-WCP-CoP composite, Fracture and Structural Integrity, 60, pp. 283-290. DOI: 10.3221/IGF-ESIS.60.20.

[20] Marwa, K.Q., Adnan, I.M., and Muhsin, J.J. (2024). Comparative study on the formability of Aluminum 1100 and Brass CuZn37 in SPIF, Engineering and Technology Journal, 42(12), pp. 1456-1473. DOI: 10.30684/etj.2024.151769.1784.